Experimental Investigation of V2I Radio Channel in an Arched Tunnel

M. Yusuf[1], E. Tanghe[1], L. Martens[1], P. Laly[2], D. P. Gaillot[2], M. Liénard[2], P. Degauque[2], and W. Joseph[1]
[1]IMEC-WAVES, Ghent University, Ghent, Belgium
[2]IEMN-TELICE, University of Lille, Lille, France

***Abstract*—This paper describes the results of the experimental radio channel sounding campaign performed in an arched road tunnel in Le Havre, France. The co-polar and cross-polar channels measurements are carried out in the closed side lane, while the lane along the center of the tunnel is open to traffic. We investigate the channel characteristics in terms of: path loss, fading distribution, polarization power ratios and delay spread. All these parameters are essential for the deployment of vehicular communication systems inside tunnels. Our results indicate that, while the H-polar channel gain attenuates slower than the V-polar channel due to the geometry of the tunnel, the mean delay spread of the H-polar channel is larger than that of the V-polar channel.**

***Index Terms*—antenna, propagation, measurement, tunnel, fading, delay spread, polarization**

I. Introduction

Vehicular communications have recently attracted much interest due to the rapid development of wireless communication technologies. Through the integration of information and communication technologies, all road users can gather sensor data and share information about traffic and road state dynamics with each other and with the road infrastructure [1]. Such traffic telematics services require reliable low-latency vehicular-to-vehicular (V2V) and vehicular-to-infrastructure (V2I) communication links that provide robust connectivity at a fair data rate. An essential requirement for the development of such vehicular systems is the accurate modeling of the propagation channel in different scenarios and environments [2].

Some V2I propagation channels resemble existing cellular links, where one node is stationary, while the other node is mobile. However, the placement height and surroundings of the infrastructure nodes for vehicular communication are unique [3]. One of the unexplored environments that needs more attention is tunnels. Being a confined environment, propagation behavior in tunnels differs from other environments as it plays the role of an oversized waveguide [4]. Deterministic channel models for tunnels include: waveguide models, ray tracing models and numerical methods for solving Maxwell's equations in tunnel environments [5]. These methods suffer from large computational complexity and incomplete description of the propagation environment. In addition, the arbitrary shape of arched tunnels makes it hard to describe its internal surface by a canonical coordinate system and, consequently, no analytical formulation is currently available [6]. While various approximate approaches have been proposed, they are more complicated to implement and the computation time may not be acceptable for long-range communication [6], [7].

On the other hand, empirical stochastic models that are obtained from measurements in real traffic condition describe the specific environment with less computational cost [5]. As the propagation is influenced by many factors (e.g. tunnel geometry, material, obstacles, Tx-Rx setup, traffic), more practical measurements are required to characterize and model the propagation in tunnels. Several measurements results have been published that investigate propagation in tunnels. Some of these studies investigate propagation in subway tunnels [8], [9], [10], where the geometry and traffic conditions are different from road tunnels. Others investigate arched tunnels in terms of only path loss [11], [12]. Authors in [13] study the field distribution in the transverse plane and the correlation in both transverse and longitudinal directions. However, these studies investigate propagation under no traffic condition and do not include dispersion parameters like delay spread as in [14]. Also, the measurement is usually carried out along the center of the tunnel.

In this work, we study the propagation of polarized channels in an arched road tunnel under real traffic conditions. The measurements are carried out in the closed lane near the tunnel wall, while the lane along the center was open for traffic. We first determine the path loss, statistical fading distributions, co-polar ratio (CPR), and cross-polar discrimination (XPD). Then, we investigate the power delay profile (PDP) and the delay spread for each polarization. Thus, the novelty of this work includes: studying the propagation in arched road tunnels under road traffic conditions, using dual-polarized wideband channel measurements near the sidewalls of the tunnel, and investigating a realistic V2I scenario, where the infrastructure node is fixed near the tunnel sidewall.

The outline of the paper is as follows: the description of measurements and methodology are presented in Section II. Section III describes the results of the analysis and discussions, while conclusions are drawn in Section IV.

II. Description of Measurements and Methodology

A. Measurement Setup and Scenario

Channel measurements are performed using the MIMOSA radio channel sounder [15]. The sounder uses dual-polarized patch antenna arrays with horizontal (H) and vertical (V)

polarizations. For this measurement campaign, uniform linear arrays of four patch antennas with 34 cm inter-element spacing (1.5 times the wavelength λ) are used at both the transmitter (Tx) and receiver (Rx), giving rise to 8 parallel Tx and Rx channels. The 8×8 sounder is fully parallel: the data from each transmit antenna is simultaneously modulated onto the carriers using interleaved frequency division multiple access. Orthogonal frequency division multiplexing (OFDM) is used to encode the digital transmit symbols. Table I summarizes the technical specifications of MIMOSA for this measurement campaign.

Measurements have been carried out in an arch-shaped road tunnel located in Le Havre, France. The tunnel has two separate tubes in opposite directions and each tube has two lanes: the lane along the center is open for traffic, while the lane on the left side is closed. Since the two tubes are identical, only one direction was investigated. This straight tunnel is 590 m long and has approximate transverse dimensions of 9.7 m width and 4.63 m height. Along the tunnel, there are lights, pipes and reflective poles as shown in Fig. 1. Two emergency exits are located on the closed lane side, with metal fence and small parking space, at one-quarter and half the distance along the tunnel.

For capturing the propagation channel along the tunnel, the Rx was mounted on the roof-top of a measurement van at a height of 2 m as shown in Fig. 1. The van moved along the closed lane with a 25 kmph speed limit. The Tx was fixed at the same height in the closed lane next to the tunnel wall, maintaining line-of-sight (LOS) with Rx. For each measurement point along the tunnel, we average the gain of all 8×8 parellel channels. Hence, we capture a channel transfer function (CTF) of size 600 snapshots × 4 polarizations × 819 subcarriers. The four polarizations are VV, VH, HV and HH, where the first polarization refers to Tx and the second to Rx.

B. Methodology of Analysis

We start our analysis by characterizing the path loss inside the tunnel, along with the CPR and XPD. Then, small-scale fading that influences the system performance is investigated. Finally, we calculate the PDP and estimate the RMS delay spread along the tunnel. Throughout our analysis, we compare these parameters for different polarizations.

Path loss: We calculate the average channel power gain $P(d)$ by averaging the power gain over all the antennas and the 819 frequency subcarriers for each polarization as a function of distance. According to [16], for tunnels of this range, a single slope model can be adapted in case of road traffic conditions. We have also tried the 2-slope model and found the single slope model to have a better agreement with the data. As a result, we use the following expression to model the average path loss in dB

$$\mathrm{PL}\,(d) = \mathrm{PL}_0 + n_{\mathrm{PL}}\ 10\ \log_{10}(d) \tag{1}$$

where $\mathrm{PL}\,(d)$ is the predicted average path loss at distance d from Tx, PL_0 is the reference attenuation, and n_{PL} is the path loss exponent. These parameters have been determined by minimizing the mean squared error between the model and the measurements.

Fig. 1. Cross-section of the tunnel with Tx in the closed lane (left) and Rx in the open lane (right)

TABLE I
MIMOSA SPECIFICATIONS

Parameter	Setting
center frequency	1.35 GHz
bandwidth	80 MHz
number of Tx and Rx antennas	4
Tx and Rx polarization	H/V
number of OFDM subcarriers	6560
OFDM symbol duration T_S	81.92 μs
cyclic prefix duration T_{CP}	$0 \leq T_{CP} \leq T_S$
full channel acquisition time	$2\,(T_S + T_{CP}) \leq 327.68$ μs

CPR: The co-polar ratio is the power ratio between the two co-polar channels gains namely VV and HH, given by the following formula in dB

$$\mathrm{CPR}\,(d) = 10\ \log_{10}\left(\frac{P\,(d)_{VV}}{P\,(d)_{HH}}\right) \tag{2}$$

where $P\,(d)$ is the averaged channel power gain received at distance d from Tx.

XPD: The cross-polar discriminator is the power ratio between a co-polar channel gain and the corresponding cross-polar channel gain. It shows the amount of depolarization that each of the two H-polar and V-polar channels goes through.

Fading distribution: In order to analyze the fading along the tunnel, we remove the path loss effect in (1) from the average channel power gain $P(d)$. Then, we calculate the local mean channel gain using a sliding average window of 40 λ and use it to normalize the average channel gain, in order to separate the small-scale fading from the large-scale fading. As a result, the scaling factor $N(d)$ applied to the average channel gain $P(d)$ in order to deduce the small-scale fading can be expressed as

$$N(d) = \frac{PL(d)}{\frac{1}{2L}\sum_{d-L}^{d+L} PL(d')P(d')} \tag{3}$$

where 2L is the 40λ window around the distance point d and $PL(d)$ is the mean path loss from (1) in linear ratio. The

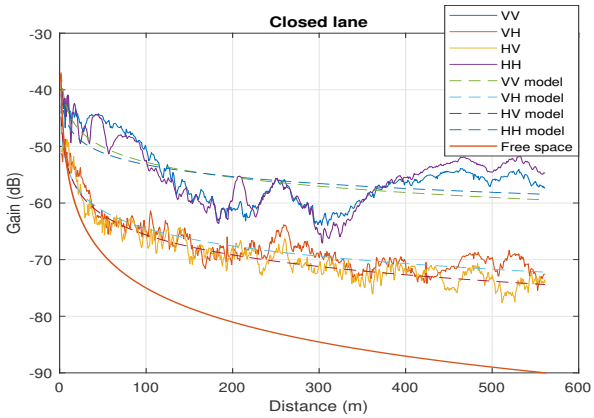

Fig. 2. Average channel gain and the deduced model for the closed lane

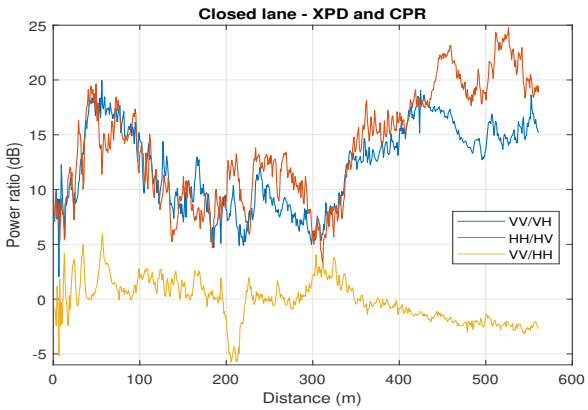

Fig. 3. XPD and CPR versus distance for the closed lane

fading distribution is acquired by calculating the histogram of the channel gain amplitude over the tunnel distance and comparing it to the classical fading distributions like Gaussian (normal), lognormal, Rayleigh, and Rician in order to decide the best fitting distribution using the Kolomogorov-Smirnov (KS) test.

RMS delay spread: In order to investigate the wideband characteristics of the channel, we determine the PDP along the tunnel by taking the inverse Fourier transform of the CTF and calculating the power of each delay component. The CTF at each distance point is first averaged over all the antennas, normalized by multiplying by $\sqrt{N(d)}$ from (3), and then windowed using a Hanning window before applying the transform. The amount of time dispersion in the tunnel can be expressed by

$$\tau_{rms}(d) = \sqrt{\frac{\sum \tau^2 P(d,\tau)}{\sum P(d,\tau)} - \left(\frac{\sum \tau P(d,\tau)}{\sum P(d,\tau)}\right)^2} \qquad (4)$$

where $\tau_{rms}(d)$ is the RMS delay spread calculated at distance d from Tx and $P(d,\tau)$ is the power component received after delay τ at distance d. In order to avoid spurious and noise components, we decide on a power threshold below which we set all the components to zero. The threshold is chosen to be 5 dB above the noise level.

III. Results and Discussion

A. Path Loss, CPR and XPD

The path loss is deduced from the CTF by averaging the power gain over all antennas and frequencies. As mentioned in the previous section, a one-slope model is used to characterize the path loss of the tunnel. Fig. 2 plots the measured channel gain $P(d)$ of different polarizations versus distance for the closed lane. The corresponding curves for the deduced models are also plotted along with the free space model. Table II summaries the model parameters in (1) for different polarizations, where the standard deviation σ_{PL} of the measured gain from the predicted model values has been added to indicate the level of large-scale fluctuation in dB.

TABLE II
Path Loss Parameters

	VV	VH	HV	HH
PL_0	34.97	43.81	42.15	39.10
n_{PL}	0.89	1.03	1.17	0.70
σ_{PL}	3.76	1.70	1.36	4.42

The power ratios between polarizations are shown in Fig. 3. Both CPR (VV/HH) and XPD (VV/VH and HH/HV) are plotted versus distance. The mean CPR over distance is 0.27 dB and the mean XPD of H-polar channel is larger than that of V-polar channel (16.7 dB compared to 13.7 dB, respectively).

These results show that the guiding effect of the tunnel results in a smaller path loss exponent than typical outdoor and indoor environments [17]. From Table II, we notice that the attenuation rate of H-polar channel is less than V-polar channel (0.7 compared to 0.89, respectively). This comes from the fact that the wave polarized normal to the plane of incidence is more reflected than the one polarized parallel to the plane of incidence, in a phenomenon known as the Brewster's angle. Since the geometry of the tunnel is such that the width is larger than the height, the H-polar wave reflected from the ground and ceiling are more than the V-polar one reflected from the walls of the tunnel, which is also observed in previous studies [6], [18]. This explains the decrease in CPR that can be seen at far distances from Tx.

On the other hand, XPD does not drop at far distances and the waves stay highly polarized, confirming previous results [7], [19]. This can be related to Table II, where the co-polar channels have smaller reference attenuation and path loss exponent than the cross-polar channels. Indeed, the ray theory of propagation in tunnels predicts that depolarization only happen at small range, where the waves impinging the tunnel walls are not polarized along the direction parallel or perpendicular to the plane of incidence [20]. At large distances, only the rays reflecting with a grazing angle, polarized along these directions, play a leading part in the propagation and thus no depolarization occurs [7]. Also, if the difference between H and V reflection coefficients is large, the depolarization

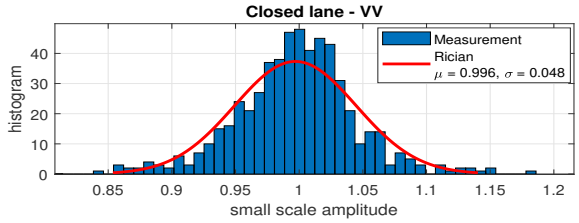

(a)

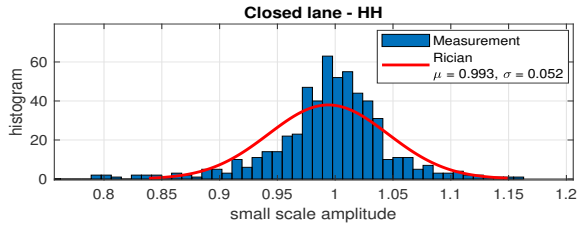

(b)

Fig. 4. Rician best fit distribution for the measurements of the closed lane for (a) V-polar channel and (b) H-polar channel

TABLE III
MEAN RMS DELAY SPREAD

	VV	VH	HV	HH
$\overline{\tau}_{rms}$ (ns)	12.94	22.17	23.57	15.35

increases and the XPD drops. This difference is largest for medium angles of incidence, which explains the drop in the XPD at the equivalent medium distances of the tunnel.

B. Fading Distributions

In tunnels, the field fluctuations are mainly related to the richness in terms of propagating modes. Indeed, a higher number of propagating modes with significant power gives rise to a higher fluctuating field [7]. The field fluctuations depend on the difference between the phases of the propagation constants associated with each mode, which leads to large pseudo-periods with distance on the large scale. The value of the pseudo-period depends on the tunnel geometry and increases with frequency and when the antenna position along the tunnel shifts from the center towards the sides of the tunnel [7]. According to [7] and [21], the pseudo-period of our scenario should approach the same order of the total tunnel range. This may explain the large-scale fading behavior of the co-polar channels shown in Fig.2.

In order to measure the small-scale fading, we remove the large-scale variations by normalizing the channel gain with respect to the local mean values. Fig. 4 shows the histogram of the small-scale fading measurements of the co-polar channels and the best fitted model according to the KS test. Indeed as reported in [22] and [23], the Rician distribution appears to best fit the experimental results. As shown in the figures, the distribution of the V-polar channel fading appears to be similar to that of the H-polar channel.

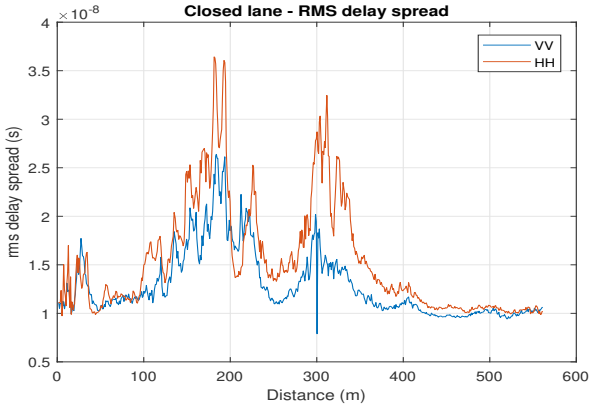

Fig. 5. RMS delay spread along the closed lane

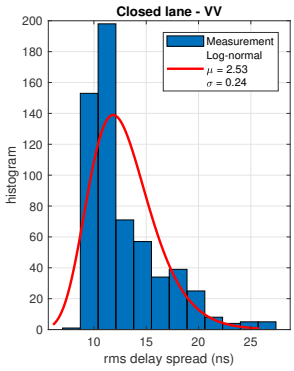

(a)

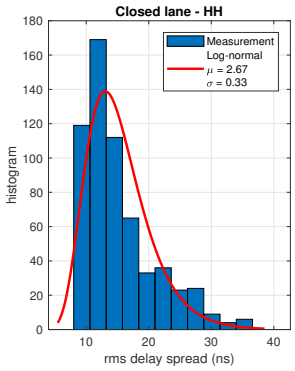

(b)

Fig. 6. RMS delay spread in the closed lane for (a) V-polar channel (b) H-polar channel

C. Delay Spread

We measure the time dispersion along the tunnel by calculating the RMS delay spread. We first deduce the PDP as mentioned in Section II, then we calculate the RMS delay spread for different polarizations after applying the threshold. Fig. 5 plots the RMS delay spread versus the distance for the co-polar channels. It is observed that, at the beginning, the delay spread slightly increases as the distance increases. After a certain distance, the higher order modes are attenuated in the far region and fewer modes are left and, as a result, the delay spread decreases again [18], [24]. However, we notice the local increase in RMS spread at almost one quarter and half the tunnel range. This can be related to the two emergency exit areas located at the same distances along the tunnel.

To decide on the distribution of the RMS delay spread, we again use the KS test to compare it with theoritical distributions. We find the best fit to be a lognormal distribution [25], shown in Fig. 6. Table III lists the mean RMS spread values along the tunnel. They are relatively larger than the values found in [14], since our scenario represents larger frequency, tunnel geometry, obstacles and traffic conditions. It can be observed that the cross-polar channels have larger

average spread than the co-polar channels, while the H-polar channel spread is larger than the V-polar channel. This can be again related to the Brewster angle phenomenon, where the width of both the tunnel and vehicles being larger than the height allows for stronger reflections of the H-polar rays compared to V-polar rays [24].

IV. Conclusion

Accurate characterization of radio propagation in tunnels is needed, specially under real traffic conditions and arbitrary shapes like arched tunnels. In this paper, results from a polarized channel sounding campaign at 1.35 GHz in Le Havre arched road tunnel have been reported. We investigated channel parameters related to path loss, fading, and time dispersion. Our analysis shows that:

- A single-slope model describes well the attenuation in a tunnel with this range under road traffic conditions. The guiding effect of the tunnel results in a path loss exponent smaller than typical indoor and outdoor environments.
- Waves are highly polarized even at far distances, with a measured XPD of about 13 dB. The geometry of the tunnel results in the H-polar waves attenuating slower than the V-polar waves, as long as the width of the tunnel is larger than its height.
- The small scale fading amplitude is found to match a rician distribution since we have LOS scenario. No much difference is observed between H-polar and V-polar channels distributions.
- RMS delay spread remains around the mean values, with a small rise at the middle of the tunnel. Mean values are in the range of 12 ns to 24 ns, with the H-polar channel spread being larger than V-polar channel spread.
- The distribution of the spread variation along the tunnel can be fitted to a log-normal distribution, with a larger standard deviation in the H-polar channel than in the V-polar channel.

Acknowledgment

This research was supported by the VLAIO project Smart Highway and the EOS project MULti-Service WIreless NETwork (MUSE-WINET).

References

[1] Intelligent Transport Systems (ITS); Vehicular Communications; Basic Set of Applications; Definitions, ETSI TR 102 638 V1.1.1, Tech. Rep., 2009.

[2] A. F. Molisch, F. Tufvesson, J. Karedal, and C. F. Mecklenbrauker, "A survey on vehicle-to-vehicle propagation channels," *IEEE Wireless Communications*, vol. 16, no. 6, pp. 12–22, 2009.

[3] W. Viriyasitavat, M. Boban, H.-M. Tsai, and A. Vasilakos, "Vehicular communications: Survey and challenges of channel and propagation models," *IEEE Vehicular Technology Magazine*, vol. 10, no. 2, pp. 55–66, 2015.

[4] D. G. Dudley, M. Lienard, S. F. Mahmoud, and P. Degauque, "Wireless propagation in tunnels," *IEEE Antennas and Propagation Magazine*, vol. 49, no. 2, pp. 11–26, 2007.

[5] A. Hrovat, G. Kandus, and T. Javornik, "A survey of radio propagation modeling for tunnels," *IEEE Communications Surveys & Tutorials*, vol. 16, no. 2, pp. 658–669, 2014.

[6] J. Molina-Garcia-Pardo, M. Lienard, P. Stefanut, and P. Degauque, "Modeling and understanding mimo propagation in tunnels," *Journal of Communications*, vol. 4, no. 4, pp. 241–247, 2009.

[7] J. Molina-Garcia-Pardo, M. Lienard, A. Nasr, and P. Degauque, "On the possibility of interpreting field variations and polarization in arched tunnels using a model for propagation in rectangular or circular tunnels," *IEEE Transactions on Antennas and Propagation*, vol. 56, no. 4, pp. 1206–1211, 2008.

[8] M. Lienard, "Mimo channels in tunnels: experimental approach and stochastic model," in *Telecommunications, 2003. ICT 2003. 10th International Conference on*, vol. 2. IEEE, 2003, pp. 1531–1535.

[9] M. Lienard, P. Degauque, J. Baudet, and D. Degardin, "Investigation on mimo channels in subway tunnels," *IEEE Journal on Selected Areas in Communications*, vol. 21, no. 3, pp. 332–339, 2003.

[10] J. A. Valdesueiro, B. Izquierdo, and J. Romeu, "On 2x2 mimo observable capacity in subway tunnels at *c*-band: An experimental approach," *IEEE Antennas and Wireless Propagation Letters*, vol. 9, pp. 1099–1102, 2010.

[11] T.-S. Wang and C.-F. Yang, "Simulations and measurements of wave propagations in curved road tunnels for signals from gsm base stations," *IEEE Transactions on Antennas and Propagation*, vol. 54, no. 9, pp. 2577–2584, 2006.

[12] A. Hrovat, G. Kandus, and T. Javornik, "Four-slope channel model for path loss prediction in tunnels at 400 mhz," *IET microwaves, antennas & propagation*, vol. 4, no. 5, pp. 571–582, 2010.

[13] J. Molina-Garcia-Pardo, M. Lienard, and P. Degauque, "Propagation in tunnels: Experimental investigations and channel modeling in a wide frequency band for mimo applications," *EURASIP Journal on Wireless Communications and Networking*, vol. 2009, p. 7, 2009.

[14] C. Garcia-Pardo, J.-M. Molina-García-Pardo, M. Lienard, D. P. Gaillot, and P. Degauque, "Double directional channel measurements in an arched tunnel and interpretation using ray tracing in a rectangular tunnel," *Progress In Electromagnetics Research*, vol. 22, pp. 91–107, 2012.

[15] P. Laly, D. P. Gaillot, M. Liénard, P. Degauque, E. Tanghe, W. Joseph, and L. Martens, "Flexible real-time mimo channel sounder for multidimensional polarimetric parameter estimation," in *Antenna Measurements & Applications (CAMA), 2015 IEEE Conference on*. IEEE, 2015, pp. 1–3.

[16] M. Liénard, S. Bétrencourt, and P. Degauque, "Propagation in road tunnels: a statistical analysis of the field distribution and impact of the traffic," in *Annales des télécommunications*, vol. 55, no. 11-12. Springer, 2000, pp. 623–631.

[17] B. M. Donlan, D. R. McKinstry, and R. Buehre, "The uwb indoor channel: large and small scale modeling," *IEEE Transactions on Wireless Communications*, vol. 5, no. 10, pp. 2863–2873, 2006.

[18] S. Bashir, "Effect of antenna position and polarization on uwb propagation channel in underground mines and tunnels," *IEEE Transactions on Antennas and Propagation*, vol. 62, no. 9, pp. 4771–4779, 2014.

[19] J. Molina-Garcia-Pardo, M. Lienard, P. Degauque, C. Garcia-Pardo, and L. Juan-Llacer, "Mimo channel capacity with polarization diversity in arched tunnels," *IEEE Antennas and Wireless Propagation Letters*, vol. 8, pp. 1186–1189, 2009.

[20] D. A. McNamara, C. W. I. Pistorius, and J. A. G. Malherbe, *Introduction to the Uniform Geometrical Theory of Diffraction*. Artech House, 1990.

[21] C. Rizzo, F. Lera, and J. L. Villarroel, "Transversal fading analysis in straight tunnels at 2.4 ghz," in *ITS Telecommunications (ITST), 2013 13th International Conference on*. IEEE, 2013, pp. 313–318.

[22] D. Didascalou, J. Maurer, and W. Wiesbeck, "Subway tunnel guided electromagnetic wave propagation at mobile communications frequencies," *IEEE Transactions on Antennas and Propagation*, vol. 49, no. 11, pp. 1590–1596, 2001.

[23] S. Loredo, A. del Castillo, H. Fernández, V. M. Rodrigo-Peñarrocha, J. Reig, and L. Rubio, "Small-scale fading analysis of the vehicular-to-vehicular channel inside tunnels," *Wireless Communications and Mobile Computing*, vol. 2017, 2017.

[24] Z. Sun and I. F. Akyildiz, "Channel modeling and analysis for wireless networks in underground mines and road tunnels," *IEEE Transactions on communications*, vol. 58, no. 6, 2010.

[25] L. Bernadó, A. Roma, A. Paier, T. Zemen, N. Czink, J. Karedal, A. Thiel, F. Tufvesson, A. F. Molisch, and C. F. Mecklenbrauker, "In-tunnel vehicular radio channel characterization," in *Vehicular Technology Conference (VTC Spring), 2011 IEEE 73rd*. IEEE, 2011, pp. 1–5.